Research Article

CMAS deposition rate and sequence effects on cyclic life in gradient testing

Byung-gun Jun[1] · Nils Jonsson[1] · Eric H. Jordan[2] · Ryan C. Cooper[2]

Received: 29 December 2022 / Accepted: 27 March 2023
Published online: 13 April 2023

Abstract
Thermal barrier coating (TBC) resistance to varied CMAS deposition rates was experimentally assessed using a temperature gradient rig using a CMAS precursor spray. TBCs were composed of EB-PVD YSZ. Five different deposition rates were tested quantifying life versus deposition rate. A high deposition rate and low deposition rate were selected from those tests for sequence testing. For sequence effect testing CMAS deposition occurred at the initial rate until the expected half-life and then switched to the other rate until failure, in the order of high deposition rate first followed by low deposition rate and vice versa. The results suggest that the order of deposition rates can affect ultimate failure behavior. Specifically applying the CMAS at the low deposition rate extended the life of the sample by a nearly a factor of 2 compared to a virgin sample. At the high deposition rate, the CMAS infiltrated all the way to the bond coat past the estimated freeze line. Data showing the coating life versus CMAS deposition rate and the existence of sequence effects in CMAS dosing are fundamentally important to coating life prediction.

Keywords CMAS resistance · Thermal barrier coating · Gradient rig · Yttria stabilized Zirconia · Deposition rate · Sequence effects

1 Introduction

Thermal barrier coatings (TBCs) are the ceramic layers applied to gas turbine hot section parts to lower metal temperatures and are an essential part of the modern gas turbine [1–4]. The insulation provided allows engines to run at higher temperatures and reduce cooling air usage, both of which improve engine efficiency. Currently, there is an ever-present drive to increase firing temperatures to further improve efficiency. A resulting side effect is the melting of ingested minerals, primarily calcium magnesium alumino silicates (CMAS), which stick on the TBCs causing coating damage [5, 6].

Several types of tests are conducted in studying TBC failure. Among those, the most engine relevant tests aim to duplicate, to a practical extent, the conditions a coating sees during service. These conditions include temperature cycling, the presence of thermal gradients, the gradual application of CMAS, variations in temperature-time cycle, and variations in CMAS accumulation rates during the history of a single component. Running tests reproducing all these factors accurately is difficult and expensive. As a result, testing conditions are simplified in order to obtain specific information. In any such testing there may be different goals that include (1) Assessing the relative durability of different coating compositions and microstructures. (2) Understanding the degradation mechanisms. (3)

✉ Byung-gun Jun, byung.jun@uconn.edu; Nils Jonsson, nils.jonsson@uconn.edu; Eric H. Jordan, eric.jordan@uconn.edu; Ryan C. Cooper, ryan.c.cooper@uconn.edu | [1]Department of Materials Science and Engineering, School of Engineering, University of Connecticut, Storrs, CT 06269, USA. [2]Department of Mechanical Engineering, School of Engineering, University of Connecticut, Storrs, CT 06269, USA.

Providing input for engineering predictions of durability in turbine hardware. This paper concerns mostly points 2 and 3 in consideration of non-constant rates of CMAS application and associated durability consequences. Nearly all published testing has used a constant and repeated thermal cycle.

It is important to note that military aircraft often fly missions that involve a wide range of throttle excursions within a given mission and between different missions. In commercial aviation, it is not uncommon for an aircraft to be shifted from one set of destinations to another, especially due to weather disruptions. Even absent weather issues, commercial aircraft can, in a single day, fly to shorter and longer destination airports with different altitudes and temperatures, leading to inconsistent flight duration and throttle demands. Thus, it is more so the rule and not the exception, that variations in temperature, time, and CMAS accumulation occur in service.

The most common type of testing due to its usefulness and comparative simplicity is constant maximum and minimum temperature and frequency furnace testing, with a representative few listed here [7–11]. Additionally, for furnace testing, one example of non-repeated block loading shows that simple linear damage rules without sequence effects worked well for temperature variation but not for cycle duration [12]. A further higher level of realism can be provided by gradient testing [13]. In this work and elsewhere [14, 15] gradient testing by torch heating is used and CMAS is applied on each cycle via a CMAS precursor sprayed onto the surface. Important constant condition testing has been done with these rigs.

In this paper, we describe testing done in a gradient heating test rig developed as a variation to the rig in Ohio State University [14] and many details of the rig can be found there. As is most relevant, the conditions of the sample will be fully described. The mission of this testing was to determine life as a function of CMAS deposition rate and to see if there are history or sequence effects with respect to non-uniform CMAS application rates. A wide variety of test plans are possible, but here we start with the simplest, which is block tests with 2 rates of CMAS application changed at the expected half-life.

2 Experimental procedure

Experiments were done on 24.5 mm diameter by 3 mm thick current state of the art bill of materials, gamma prime single crystal super alloy buttons with an LPPS MCrAlY bond coat and a 120 micron thick Electron Beam Physical Vapor (EB-PVD) yttria stabilized zirconia (YSZ) TBC on them. These button samples were tested on the University of Connecticut's thermal gradient rig with preset thermal cycles. The thermal gradient rig is an improved version of that in [14] and uses an oxygen propane flame for heating and forced air backside and front side cooling,

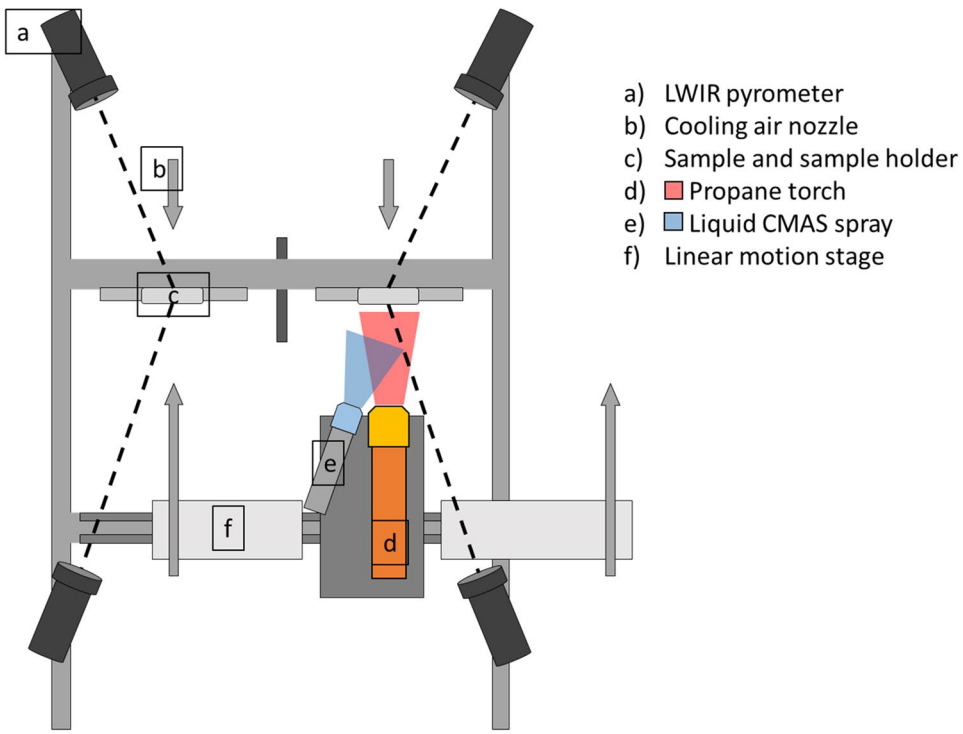

Fig. 1 Rough schematic of gradient rig testing setup. Long wavelength infrared pyrometers are directed at the front (TBC) and back (superalloy) of the sample. An aerosolizing spritzer sprays liquid nitrate based CMAS at the sample during sample heating. A moving stage moves the propane-oxygen torch, CMAS spritzer, and front-side air cooling nozzles from one sample to the other

a schematic of which is provided in Fig. 1. The torch used was a surface mixed glass blowing torch (Norton Red Max). The front and back side temperatures are measured using long wavelength (8–14 microns) pyrometers. TBCs tend to be both translucent in the mid IR and have spectrally non uniform emissivity [16] and as a result, long wavelength pyrometers are needed to get sensible surface temperature measurements.

Emissivity changes due to oxidation of the substrate superalloy back surface was compensated for by spraying the superalloy with high-temperature paint (VHT Flameproof Coating) with a known emissivity. This paint generally does not survive the full cyclic test, but the rig is programmed to run at a constant, mass flow regulated gas flow. Thus, the rig maintains approximately constant heat flux such that the loss of the paint late in the test will not change operating conditions. As a side note, the front side and back side temperature can change due to TBC sintering or coating loss however operating gas turbines will not be able to adjust heat flux alongside such changes. It is therefore more realistic to run the rig at constant gas flow as opposed to actively controlling the front and/or back side temperatures.

Two samples were tested simultaneously in the rig. The torch and front side cooling jets move between two sample stations such that the hot time of one sample is the cooling time of the other. The thermal cycle was set at 2 min to ramp up to the target front side temperature of 1250 °C and 4 min of hot time at the target temperature. The back side is cooled continuously by a cooling air jet. The backside temperature is nearly steady state at 950 °C during the hold time. The propane and oxygen flow rates are controlled by mass flow controllers. The gas flow required to meet the target temperatures are adjusted prior to the start of the test and is programmed into the mass flow controllers. The mass flows are constant during the remainder of the test. Failure was determined from a video recording of every cycle defined as the point of 50% coating delamination, and cycling was stopped as soon as failure was discovered by the operator. Failure criteria was seen to have been met rapidly (within a small fraction of total survived cycles) after minor initial delamination. Front and back side temperatures are measured and recorded continuously. The front side of the sample is constantly monitored and recorded by video camera, allowing the operator to determine failure life after testing without having to observe every cycle and to determine if the failure occurs during heating or cooling. Samples were observed to fail during cooling.

A CMAS solution is utilized to correspond to AFRL03 using dissolved nitrates for all cations except Si which was provided by a colloidal suspension. Chlorides were provided with NaCl and sulfates were introduced with L-cystine. Carbonates were not provided given that dolomite, the sole source of carbonate in AFRL 03, when heated to 700 °C ~ 850 °C undergoes calcination, removing the carbonates from the system far below both the melting temperature of AFRL 03 at 1176 °C, and the front side temperature of our testing at 1250 °C. All chemicals are 98% pure. The composition of AFRL 03 is shown in Table 1. Five mL of CMAS solution is sprayed on the sample at the beginning of every cycle during heating, when the TBC reaches approximately 600 °C. Previous experiments proved that the CMAS solution did not infiltrate as a water-based solution but remained on the surface until it infiltrated as a melt. A small temperature dip is recorded as the solution is applied at an intermediate temperature during heating. Experiments in which an equivalent amount of deionized water was applied showed that the thermal shock of the solution application had negligible impact on cyclic life. The CMAS application rate is controlled by the weight% of CMAS in the spray solution. Solution concentrations were 1/8, ½, 1, and 2 wt% of equivalent oxides with the 1/8 wt% and 2 wt% concentrations being used as the low and high concentrations respectively. An approximated CMAS capture ratio of 10% was applied to the deposition rate calculations in this paper. To determine the capture ratio, a TBC button was weighed before and after 100 mL of 2 wt% CMAS was sprayed. The process was repeated several times to a total of 500 mL of CMAS solution sprayed. Because the weight change from capture could be affected by oxidation growth or local spallation, CMAS spray occurred during heating as per a standard testing

Table 1 Melting points, composition, and distribution of minerals in AFRL 03. *Decomposition of dolomite begins around 300 °C but melting of MgO occurs at 2850 °C and melting of CaO occurs at 2550 °C

Mineral	Melting Point	Chemical composition	Distribution (%)
Quartz	1670 ~ 1713 C	SiO_2	34
Gypsum	1460 C	$CaSO_4$	30
Aplite	~ 1200 C	$SiO_2 + KAlSi_3O_8$-$NaAlSi_3O_8$-$CaAl_2Si_2O_8$	17
Dolomite	2900 C*	$CaMg(CO_3)_2$	14
Salt	800 C	NaCl	5

cycle, but the time spent at the target temperature was minimized.

CMAS concentration lifetime tests were run with 4 samples per condition in order to determine cyclic life versus CMAS deposition rate and provide baselines for each concentration. Cumulative damage lifetime tests were done under a high deposition rate followed by a low deposition rate (High-Low) and low rate followed by a high rate (Low–High) test condition. Under both conditions, the sample was subjected to the first concentration for a number of thermal cycles equal to 50% of that respective single concentration lifetime. Then, the sample was tested until failure on the subsequent concentration. Finally, interrupted lifetime testing was done for single CMAS concentration conditions. Samples were cycled under a simple low rate or high rate condition until half of their expected lifetimes, before any visible signs of degradation was apparent, then removed for imaging. 4 samples were tested for every test condition, with each condition being repeated twice with two samples per test.

Upon failure or interruption, all samples were imaged with the Aspex Explorer SEM for a detailed surface map. Then, the samples were mounted in epoxy, cut, remounted, and imaged again at a higher resolution. SEM imaging and EDS mapping were done using a Teneo LoVac SEM. Samples were provided by an OEM sensitive to lifetime data and TGO/substrate data. Lifetime and interrupted cycle times were normalized against the lifetime of a baseline TBC subjected to the same thermal cycle without CMAS. Micrographs have been edited to remove depictions of the YSZ/TGO/Bond coat interface at the request of our industrial sponsor. In addition, the actual cyclic lives and TGO images from which life can be estimated cannot be released nor can the sponsors be identified.

3 Results

3.1 CMAS deposition rate testing

CMAS deposition rate trials utilizing the AFRL 03 water-based solution precursor on YSZ button samples were done. The effect of CMAS deposition rate on the normalized TBC lifetime is summarized in Fig. 2 as the solid descending blue line. The average lifetime was found across each sample and normalized by dividing the life of each sample by the cyclic life of a baseline sample with no CMAS. This normalization of cyclic life is used consistently throughout this paper. Normalized standard deviation was found to be under 3% for all test conditions. Increasing CMAS deposition rates were shown to decrease the lifetime of the TBC strongly. The total CMAS deposited to yield failure, shown as the orange solid line, is shown to increase until the 0.8 mg of oxide/min deposition rate. After which, at the next higher CMAS deposition rate, the total CMAS deposited to cause failure decreases. The calculated amount to fully infiltrate the porosity (10%) is 6.5 mg. On this basis the CMAS needed to fill all the porosity in the coating is well exceeded at failure in all the tests run. Therefore, we can remove the potential lack of CMAS as a limiting condition for final failure.

Figures 3 and 4, and 5 show SEM images of cross-sections of the 0.1 mg of oxide/min, 0.8 mg/min, and 1.6 mg/min samples, respectively labelled as Low, Medium, and High deposition rate samples. Note that the TGO and bond coat is not shown at the request of the sample provider. Each cross section contains markings with apparent infiltration depths, with the Low and Medium rate samples showing CMAS arresting at certain points within the sample and the High deposition rate samples showing full infiltration. The infiltration depths alongside normalized lifetime and deposition rates are indicated in Fig. 6. All lifetimes and cycle times are normalized against the

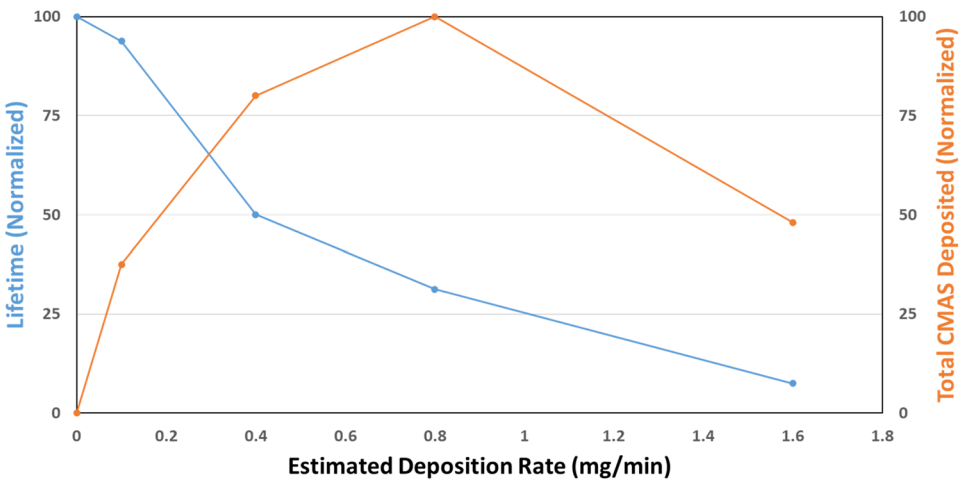

Fig. 2 Summarized results of CMAS deposition rate effects on TBC lifetime. Solid blue lines indicate experimental results. Cycling data is normalized against the lifetime of a TBC subjected to the same thermal profile without CMAS. The orange line shows CMAS accumulation data which is normalized against the largest amount of CMAS deposited between the trials

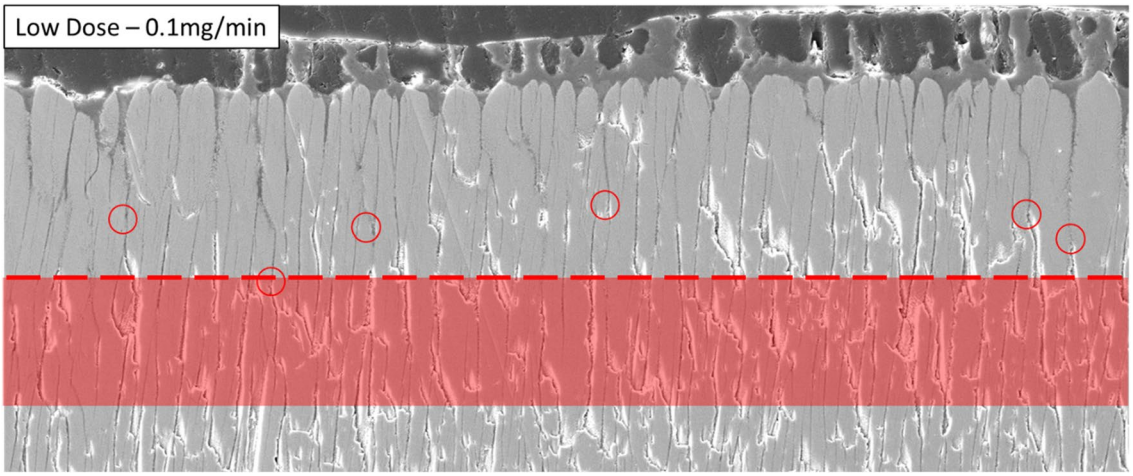

Fig. 3 Cross-section of low deposition rate condition (0.1 mg/min) with several CMAS freeze locations circled in red. Dotted line indicates initial theoretical freeze line. Translucent band indicates potential movement of freeze line with CMAS infiltration

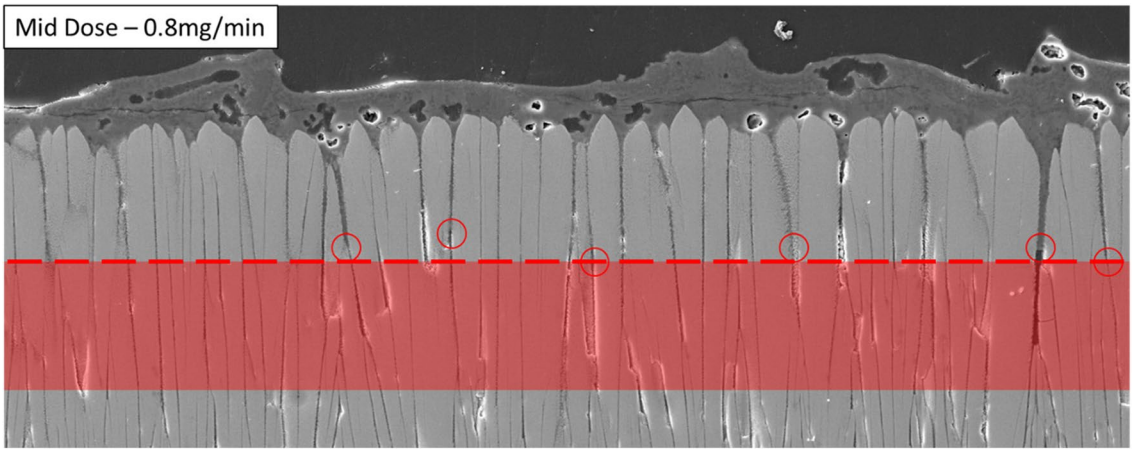

Fig. 4 Cross-section of medium deposition rate condition (0.8 mg/min) with several CMAS freeze locations circled in red. Dotted line indicates initial theoretical freeze line. Translucent band indicates potential movement of freeze line with CMAS infiltration

lifetime of a sample subjected to the same thermal profile without CMAS. Delamination occurred almost exclusively at the YSZ/TGO interface in all samples, including non-CMAS baseline samples. A couple instances of delamination representing a tiny fraction of the failure surface of the TGO/bond coat interface were observed but they were only found in samples subjected to the longest cycling and only at the edge of the failed sections. We presume these instances occurred because of the exposure of the unprotected TGO to the propane torch.

To remove the possibility of CMAS infiltration post coating delamination, additional interrupted testing was done at the Low and High deposition rates up to 50% of the expected life. The resulting microscopy, as shown in Fig. 7 mirrors the results seen before in Figs. 3 and 5, with visible CMAS arrest at the low deposition rate and full infiltration at the high deposition rate. This shows that the post test infiltration depths did not occur after failure.

3.2 Mixed deposition rate testing

Cumulative damage testing was done using the Low and High deposition rates in order to determine the impact, if any, of deposition ordering. Using lifetime numbers from the deposition rate trials, experiments were set up to expose samples to 50% of the expected life under one deposition condition, and then cycle the sample until failure in the other. Both Low–High and High–Low deposition sequences were tested. The theoretical lifetime under the two conditions was derived using Miners Rule as a simplistic cumulative damage model in Eq. 1.

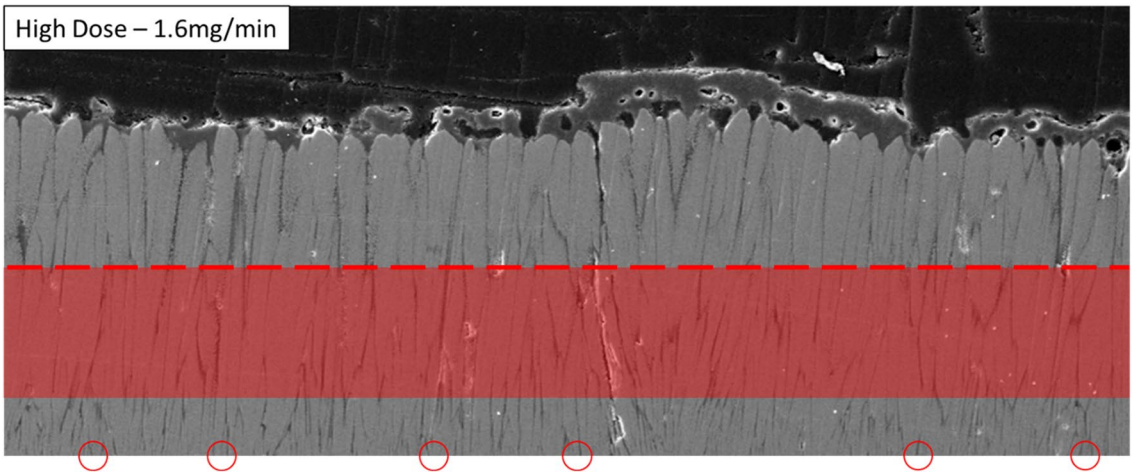

Fig. 5 Cross section of high deposition rate condition (1.6 mg/min). CMAS infiltration was complete down to the TGO which is why the freeze location circles are at the bottom of the image. Dotted line indicates initial theoretical freeze line. Translucent band indicates potential movement of freeze line with CMAS infiltration

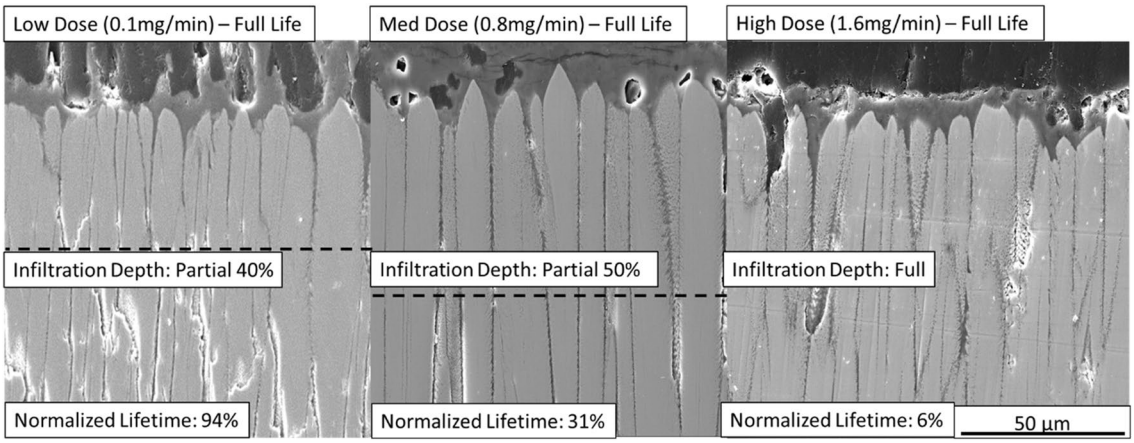

Fig. 6 Infiltration depths and normalized lifetimes by deposition rate of the low, medium and high conditions

$$1 = n_1/Nf1 + n_2/Nf_2 \quad (1)$$

n_1, n_2=number of cycles applied at conditions 1 and 2 respectively.

Nf_1, Nf_2 = number of cycles to failure in a single condition test at conditions 1 and 2, respectively.

Figure 8a shows the amount of time the samples spent in the low deposition rate condition and Fig. 8b shows the time spent at the high deposition rate condition. These cyclic time values are normalized against the lifetime of a baseline sample, as with other lifetime data. The low contrast bars in Fig. 8a and b indicate the expected lives, as derived by Miner's rule, of each condition when applied as the second condition. 8a therefore indicates the expected life under the low rate when preceded by the high rate for the first 50% of life, and 8b indicates the expected life under the high rate when preceded by the low rate for the first 50% of life. It is worth noting that the life at the high deposition rate was much longer (almost 2X) if the sample had previously been exposed at the low deposition rate compared to a virgin sample solely exposed to the high deposition rate. The significantly longer life, especially when compared to the prediction by Miner's rule, indicates a benefit of prior cycling at the low rate.

As with the single deposition rate testing, all delamination was observed to have occurred near the YSZ/TGO interface and in the topcoat. In all samples, the back scatter micrographs did not show any indication of non-alpha oxide phase formation.

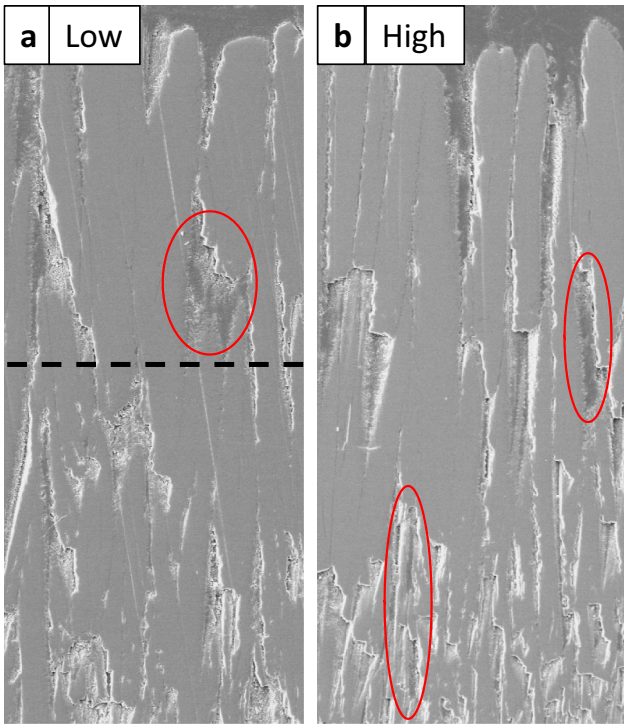

Fig. 7 CMAS infiltration depths of (**a**) Low and (**b**) High deposition rate conditions on interrupted samples. Visible sections of CMAS infiltration are circled in red. Samples were removed from testing at half their expected lifetimes and showed no signs of delamination

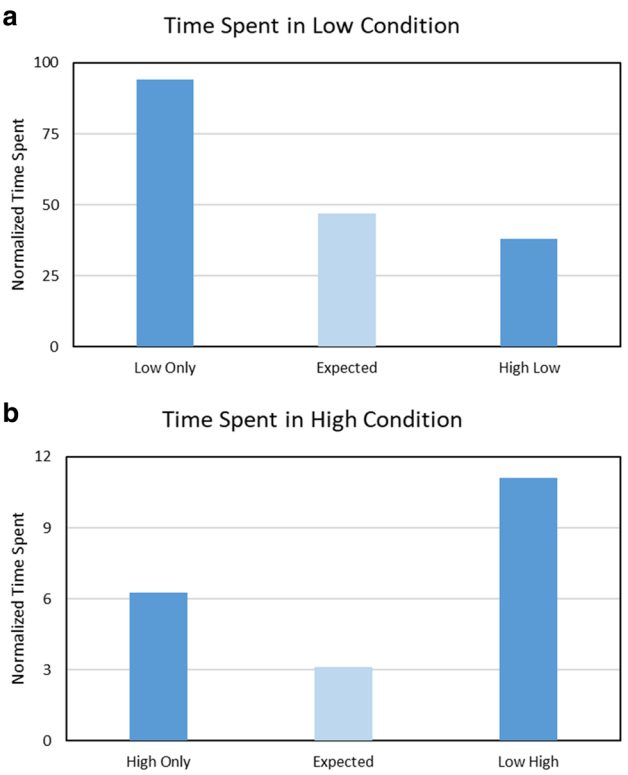

Fig. 8 Summary of time spent by each test variation in the (**a**) low deposition rate condition and (**b**) high deposition rate condition. All data is normalized against a sample with no CMAS deposition. Light blue bars indicate the expected life of the samples as predicted by the linear damage model. Dark blue bars indicate actual life of different samples under the given condition. The axis in (**b**) is adjusted for better readability

4 Discussion

TBC failure during thermal cycling can involve many mechanisms that depend on the materials used, temperature cycle profile and duration, and CMAS deposition rate, as reviewed, for example, in [17]. These failure mechanisms could include failures related to oxide behavior, bond coat rumpling, chemical attack on the TBC including hot corrosion and CMAS attack. In the present experiments, the number of cycles is all less than 1000 cycles and the hot time less than 100 hrs. No significant failure is found in the TGO layer, nor was there any formation of other oxides or new interface phases as seen in [18]. The failure in these experiments is likely to be dominated by the mechanical stiffening effects of CMAS, resulting in high stress buildup and subsequent failure as described in [19–21], where a deeper CMAS penetration depth leads to a shorter TBC lifetime.

4.1 Deposition rate dependence of CMAS infiltration and damage

In discussing CMAS damage one useful parameter is the amount of CMAS needed to fill all the porosity to full coating thickness. In the present case that would be 6.5 mg. It is observed that not all porosity is filled so the amount of CMAS needed to fill the porosity in the actual cases is less than this amount. Previously it was noted that all tests have more than 6.5 mg applied before failure. Considering that all pores might not be filled, each of these tests can be strongly considered to have surplus CMAS. The CMAS infiltration at failure, therefore, is not limited by the amount needed to fill porosity. A second consideration is the depth at which it is estimated that the temperature in the TBC drops below the freezing point of the CMAS. The CMAS melting point from previous DSC measurements is 1176 °C [22]. Assuming thermal conductivities of 0.92 W/mK for the un-infiltrated YSZ, 2.04 W/mK for infiltrated YSZ [23], and 23 W/mK for the superalloy substrate, as well as our known front/back temperatures and layer thicknesses, theoretical freeze bands were calculated using the finite difference method (FDM) of 1D transient heat transfer [24, 25]. Note that the values from the literature may differ from actual values as, for example, the infiltrated YSZ conductivity was derived using APS coatings while our coatings are EB-PVD. Nevertheless, the resulting calculations serve suitably as

a rough approximate. The dotted red line in Figs. 3 and 4, and 5 indicate the CMAS freeze depth for un-infiltrated YSZ samples. The deeper bands below indicate where the freeze line could reach with continued CMAS infiltration as the thermal conductivity changes over time. With the values above, we calculated the freeze band to range from approximately 50 ~ 70% of the full depth of the TBC.

Additionally, we calculated the theoretical freeze line of a fully infiltrated topcoat with our estimated numbers as well as the thermal conductivity required for the freeze line to end up past the TGO. With our assumed conductivities, we found the theoretical deepest freeze line to occur at 80% of the full topcoat thickness, and the required thermal conductivity of the fully infiltrated YSZ would have to be 2.7 W/mK for the freeze line to reach the TGO. Considering that fully dense 7YSZ has a conductivity of 2.5 W/mK and both amorphous and crystalline CMAS have conductivities below 2 W/mK, we can assume that the freeze line of the CMAS will never be pushed below the TGO in the samples we used. Although the freezing point of the CMAS could change due to compositional changes through dissolution of TBC elements, this phenomenon should have a larger impact with longer lifetimes. The limit of the freeze line, in combination with the short lifetimes of high deposition rate samples, supports the idea that at the high deposition rate, CMAS flows past the freeze line as a supercooled liquid.

At high deposition rates the single first dose is theoretically enough to fully infiltrate all the porosity to the full depth. Given that we know the freeze line is before the TGO, the infiltrating CMAS is likely flowing past the freeze line as a super cooled liquid. At low deposition rates, however, the scarcity of CMAS means that infiltration happens incrementally, over multiple cycles, ultimately arresting at the approximate freeze depth with a thinner layer of fully infiltrated coating. In both cases the increase in the conductivity of the TBC with infiltration increases the penetration depth and assists the flow of CMAS toward a moving freeze line. Increased CMAS infiltration depth, and subsequent TBC stiffening, is known to increase the likelihood of delamination and is consistent with the change in lifetime with deposition behavior shown in Fig. 2. The infiltration depth also explains the improvement in life of the low-high condition, as the initial low deposition rate establishes a freeze line which the subsequent high deposition rate is unable to move past.

In Fig. 6 the depth of infiltration is indicated by the dotted lines. It is apparent from the CMAS layer on the surface of the TBCs in Fig. 6, as well as the related Figs. 3, 4 and 5, and 7 that the CMAS accumulates on the surface of the TBC. At our estimated capture rate of 10%, we know that every deposition rate condition was supplied with significantly more than the requisite upper bound of 6.5 mg of CMAS for full infiltration before failure. CMAS frozen past the freeze line is not expected to melt during subsequent heating cycles barring changes in thermal conductivity of the TBC or chemistry of the CMAS melt. Even if the frozen CMAS were to melt, the viscosity of the CMAS would be so high at the freeze line that further infiltration would be incremental. The CMAS accumulation on the surface is understandable then as there is surplus CMAS being deposited even after full CMAS infiltration, and more so when the infiltration is halted at the freeze line. Although the accumulated CMAS can further change the thermal conductivity of the TBC by infiltrating more difficult to infiltrate pores, the rate is much slower due to the difference in volume of CMAS required to affect the infiltration depth.

Different deposition rates affect the rate of accumulation of CMAS. For samples with similar infiltration behavior, differences in accumulated CMAS can act as an indicator for failure life. Accumulated CMAS on the surface worsens the stress situation as it acts as an extension of the infiltrated layer [21]. As shown in Fig. 2, increasing CMAS accumulation led to decreased life in all but the highest deposition rate, consistent with what is expected. At the highest deposition rate, where there was significantly less CMAS deposited, there was full CMAS penetration, leading to reduced life as expected by models of the effects of stiffening [19–21].

The difference in CMAS availability during the early cycles seems to be the major contributing factor determining infiltration behavior. At high deposition rates, excess CMAS availability allows the possibility of full CMAS penetration in one cycle. This higher infiltration rate also changes the thermal conductivity on a larger scale. During subsequent heating cycles, the existing CMAS is more likely to remelt and in combination with the newly introduced CMAS will infiltrate further if it has not already fully infiltrated. At low deposition rates, the scarcity of CMAS from cycle to cycle prevents CMAS from penetrating as deeply during early cycles. As such, once CMAS infiltrates to or past the freeze line, it has time to freeze. In addition, the change in thermal conductivity of the TBC by infiltration is less extensive and does not push the freeze line as deep as in the high rate situation leading to a shallower final freeze line.

4.2 Order dependence of cumulative damage testing

The difference in infiltration behavior exhibited between the low and high deposition rates is a key consideration when discussing the behavior of the cumulative damage testing samples. In Fig. 8, we normalized the time spent in each deposition rate condition for each test condition against the time to failure for a sample with no CMAS as in

all other charts. Figure 8a represents the normalized lives endured at the low deposition rate, and Fig. 8b represents the normalized lives endured at the high deposition rate. The light blue bars indicate the expected life of the mixed deposition rate samples as predicted by the linear damage model. The dark blue bars are the actual times spent by a sample in the given condition.

When comparing lifetime durations in solely the high deposition rate condition, Fig. 8b most notably indicates the significant improvement in lifetime (> 2x) of the low–high sample compared to both the single high rate sample as well as the prediction by the linear damage rule. Low deposition rate cycling has extended the life under the high deposition rate. Conversely, the high–low condition has spent less time in the low condition prior to failure than expected by both the linear damage model, and as seen in the single low rate sample. These discrepancies indicate that the high rate condition has negatively impacted the TBCs resistance to subsequent low deposition rates, while the initial application of the low deposition rate was highly beneficial.

Figure 9 shows the CMAS infiltration depths of the four conditions, Low only, Low–High, High–Low, and High only. Here, we see that the CMAS infiltration behavior of the mixed rate samples follow the behavior of the initial rate. The low–high condition shows partial infiltration and CMAS freezing much like the low only condition, and the high–low condition shows full infiltration like the high only condition. If the initial deposition rate determined the infiltration behavior, the disparity between experimentation and the linear damage model can be explained.

The differences in infiltration depth serves as an explanation for the differences in lifetimes in the different conditions based on the stiffening effects of CMAS outlined in [23–25] where greater infiltration depths are more harmful. Low initial deposition limits the infiltration depth of the subsequent high deposition rate lengthening the life, while the initial high deposition rate the establishes full infiltration, lowering the life compared to the low only rate where full infiltration does not occur. A future consideration is to see if the kinetics of CMAS blocking by apatite formation in gadolinium zirconate have properties that lead to similar sequence effects.

5 Conclusion

Quantitative data on coating life as a function of CMAS deposition rate is presented which is a fundamental ingredient for life prediction. The total CMAS required for failure is not a constant but depends on CMAS deposition rate. This is fundamental information useful for life prediction. Experiments have shown that at all but the highest CMAS deposition rates, CMAS infiltration arrests in the vicinity of the freeze line as expected. For the highest CMAS deposition rate the CMAS fully infiltrates to the bond coat past the estimated freeze line. CMAS infiltration below the freeze line is consistent with the idea that at high deposition rates the CMAS may infiltrate more deeply as a super cooled liquid before freezing. Even using the upper bound conductivity of a fully infiltrated coating does not predict the freeze line reaching the TGO layer. The present results indicate that high CMAS deposition rates early in a turbines lifetime are likely to particularly detrimental. It is also observed that CMAS deposited at a low rate, with arrest near the freeze line, is beneficial to any

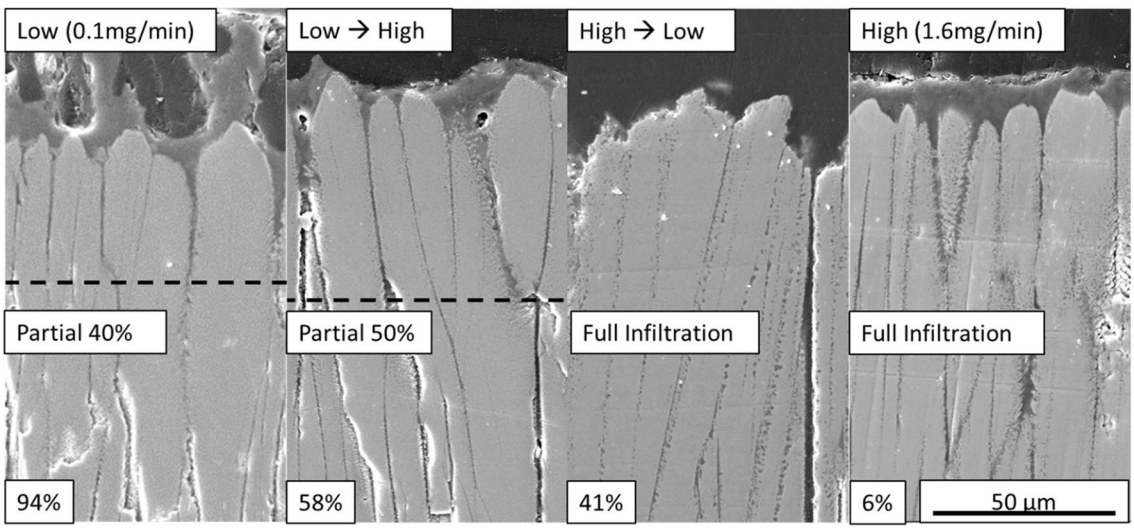

Fig. 9 CMAS infiltration depths of Low, Low to High, High to Low, and High deposition rate conditions. Labels from top to bottom are deposition condition, infiltration depth, and normalized lifetime, respectively

subsequent deposition at higher rates as the subsequent CMAS can only accumulate on the surface of the TBC. The prior establishment of a freeze line, therefore, extends the lifetime of a TBC subjected to a high deposition rate CMAS attack in the future. These deposition rate sequences affect physical behavior and results in poor predictions by Miners linear damage rule, as expected, in that Miners rule does not account for sequence effects. Although generally unacknowledged in life prediction models, recognizing the sequence effects related to CMAS deposition rate are fundamentally important.

Acknowledgements The authors would like to thank Dr. Roger Ristau and Dr. Lichun Zhang at the UConn Center for Advanced Microscopy and Materials Analysis.

Author contributions All authors contributed to the study conception and design. Material preparation and data collection was performed by BJ with assistance from NJ. Analysis was performed by BJ. The first draft of the manuscript was written by BJ and all authors commented on previous versions of the manuscript. All authors read and approved the final manuscript.

Data and code availability Data is not available for the public.

Declarations

Conflict of interest We have no conflicts of interest to disclose.

References

1. Padture NP, Gell M, Jordan EH (2002) Thermal barrier coatings for gas-turbine engine applications. Science 296:280–284. https://doi.org/10.1126/science.1068609
2. Stiger MJ, Yanar NM, Topping MG, Pettit FS, Meier G (1999) Thermal barrier coatings for the 21st century. Z Fur Met 90:1069–1078
3. Miller RA (1997) Thermal barrier coatings for aircraft engines: history and directions. J Therm Spray Technol 6:35–42. https://doi.org/10.1007/BF02646310
4. Evans AG, Mumm DR, Hutchinson JW, Meier GH, Pettit FS (2001) Mechanisms controlling the durability of thermal barrier coatings. Prog Mater Sci 46:505–553. https://doi.org/10.1016/S0079-6425(00)00020-7
5. Li L, Hitchman N, Knapp J (2010) Failure of thermal barrier coatings subjected to CMAS attack. J Therm Spray Technol 19:148–155. https://doi.org/10.1007/s11666-009-9356-8
6. Borom MP, Johnson CA, Peluso LA (1996) Role of environmental deposits and operating surface temperature in spallation of air plasma sprayed thermal barrier coatings. Surf Coat Technol. https://doi.org/10.1016/S0257-8972(96)02994-5
7. Kumar R, Jordan E, Gell M, Roth J, Jiang C, Wang J, Rommel S (2017) CMAS behavior of yttrium aluminum garnet (YAG) and yttria-stabilized zirconia (YSZ) thermal barrier coatings, surf. Coat Technol 327:126–138. https://doi.org/10.1016/j.surfcoat.2017.08.023
8. Schlichting KW, Padture NP, Jordan EH, Gell M (2003) Failure modes in plasma-sprayed thermal barrier coatings. Mater Sci Eng A 342:120–130. https://doi.org/10.1016/S0921-5093(02)00251-4
9. Xie L, Sohn Y, Jordan EH, Gell M (2003) The effect of bond coat grit blasting on the durability and thermally grown oxide stress in an electron beam physical vapor deposited thermal barrier coating. Surf Coat Technol 176:57–66. https://doi.org/10.1016/S0257-8972(03)00466-3
10. Madhwal M, Jordan EH, Gell M (2004) Failure mechanisms of dense vertically-cracked thermal barrier coatings. Mater Sci Eng A 384:151–161. https://doi.org/10.1016/j.msea.2004.05.061
11. Ahmadian S, Thistle C, Jordan EH (2013) Experimental and finite element study of an air plasma sprayed thermal barrier coating under fixed cycle duration at various temperatures. J Am Ceram Soc 96:3210–3217. https://doi.org/10.1111/jace.12552
12. Patel NV, Jordan EH, Sridharan S, Gell M (2015) Cyclic furnace testing and life predictions of thermal barrier coating spallation subject to a step change in temperature or in cycle duration. Surf Coat Technol 275:384–391. https://doi.org/10.1016/j.surfcoat.2015.04.037
13. Traeger F, Vaßen R, Rauwald KH, Stöver D (2003) Thermal cycling setup for testing thermal barrier coatings. Adv Eng Mater 5:429–432. https://doi.org/10.1002/adem.200300337
14. Gledhill AD (2011) Thermal barrier coatings chemically and mechanically resistant to high temperature attack by molten ashes. Ohio State University, Ohio
15. Mack DE, Wobst T, Jarligo MOD, Sebold D, Vaßen R (2017) Lifetime and failure modes of plasma sprayed thermal barrier coatings in thermal gradient rig tests with simultaneous CMAS injection, surf. Coat Technol 324:36–47. https://doi.org/10.1016/j.surfcoat.2017.04.071
16. Eldridge JI, Spuckler CM (2008) Determination of the scattering and absorption coefficients for plasma sprayed Yttria-Stabilized Zirconia thermal barrier coatings. J Am Ceram Soc 91:1603–1611 (**[5]**)
17. Kumar V, Balasubramanian K (2016) Progress update on failure mechanisms of advanced thermal barrier coatings: a review. Prog Org Coat 90:54–82
18. Tolpygo V, Vapor-Phase CMAS-Induced (2017) Degradation of adhesion in thermal barrier coatings. Oxid Met 88:87–96
19. Evans AG, Hutchinson JW (2007) The mechanics of coating delamination in thermal gradients. Surf Coat Technol 201:7905–7916. https://doi.org/10.1016/j.surfcoat.2007.03.029
20. Kramer S, Faulhaber S, Chambers M, Clarke DR, Levi CG, Hutchinson JW, Evans AG (2008) Mechanisms of cracking and delamination within thick thermal barrier systems in aero-engines subject to calcium-magnesium-alumino-silicate (CMAS) penetration. Mater Sci Eng A 490:26–35
21. Mercer C, Faulhaber S, Evans AG, Darolia R (2005) A delamination mechanism for thermal barrier coatings subject to calcium-magnesium-alumino-silicate (CMAS) infiltration. Acta Mater 53:1029–1039
22. Wiesner VL, Bansal NP (2015) Mechanical and thermal properties of calcium–magnesium aluminosilicate. J Eur Ceram Soc 35:2907–2914. https://doi.org/10.1016/j.jeurceramsoc.2015.03.032
23. Kakuda TR, Levi CG, Bennett TD (2015) The thermal behavior of CMAS-infiltrated thermal barrier coatings. Surf Coat Technol 272:350–356. https://doi.org/10.1016/j.surfcoat.2015.03.043

24. Panwar SS, Patro TU, Balasubramanian K, Venkataraman B (2016) High-temperature stability of yttria-stabilized zirconia thermal barrier coating on niobium alloy-C-103. Bull Mater Sci 39:321–329. https://doi.org/10.1007/s12034-015-1140-4
25. Wee S, Do J, Kim K, Lee C, Seok C, Choi BG, Choi Y, Kim W (2020) Review on mechanical thermal properties of superalloys and thermal barrier coating used in gas turbines. Appl Sci. https://doi.org/10.3390/APP10165476